POLITECNICO
MILANO 1863

SCUOLA DI INGEGNERIA INDUSTRIALE
E DELL'INFORMAZIONE

Executive Summary of the Thesis

Analysis of disposal manoeuvres design in the Laplace plane for Highly Elliptical Orbits

Laurea Magistrale in Space Engineering

Author: André Luis Dos Santos Hengemuhle

Advisor: Prof. Camilla Colombo

Co-advisor: Xiaodong Lu

Academic year: 2022-2023

1. Introduction

The exponential growth of space debris, symbolized by the *Kessler syndrome* [1] phenomenon, poses a serious threat to Earth's orbits. The danger is the generation of a cascade reaction, featuring the collisions and fragmentation of uncontrolled orbiting objects. there is an urgent need for effective mitigation strategies. Currently the Inter-Agency Space Debris Coordination Committee (IADC) guidelines primarily address Low Earth Orbit (LEO), leaving Medium Earth Orbit (MEO) and Highly Elliptical Orbit (HEO) under-regulated. Nonetheless, HEO orbits are characterised by a large eccentricity and may lead to interferences with the populated LEO region, increasing the risk of fragmentation events.

This work thus addresses the the problem of end-of-life design for HEO satellite, building upon previous works by Colombo et al. [2, 3], Scala [4], and analysing disposal manoeuvre optimisations in this region of Earth's orbits.

The main perturbation effects acting on HEO satellites are the Earth's oblateness and the lunisolar gravitational attraction. The goal of the disposal manoeuvre optimisation is to exploit the eccentricity oscillation induced by those different perturbations, to obtain a natural atmospheric re-entry.

In particular, following the work from Asperti [5] the aim is to analyse analytical-based optimisation strategies to lower the expensive computational burden of the global optimisation algorithms usually implemented. This would enable the possibility for autonomous end-of-life planning by the satellite's on-board microprocessor.

The research is based on the application of the Triple-Averaged (TA) model to study the dynamics, allowing the exploitation of the Hamiltonian formulation analytically. The computations are carried out considering various typologies of the Laplace frame.

The original contribution of this work is the proposed optimisation strategy considering the time variation of the third-bodies' ephemerides. This triggers the possibility of exploiting a rotating Laplace frame to describe the dynamics of the problem.

Additionally, a hybrid approach merging semi-analytical and analytical methods is introduced. This attempts to merge the goods of both the analytical approach and global optimisation.

2. Modelling

Considering the region where a HEO satellite operates, this work modelling takes into account the effect of the Earth's oblateness and the lunisolar attraction. Their contribution to the dynamics is computed using the associated perturbing potential $\mathcal{R}$, and are therefore employed in the orbital propagation with the Lagrange Planetary equations (see Vallado for reference [6]).
The generic expression of the third Earth's oblateness potential is:

$$R = -\frac{\mu J_2 R_\oplus^2}{2r^3}(3\sin^2\phi - 1) \tag{1}$$

where μ and $R_\oplus$ are respectively the Eatrh's gravitational parameter and radius, r is the satellite's distance to the centre of the planet, J_2 is the second order harmonic Earth's geopotential coefficient and ϕ is the satellite's latitude over the equator.
The third-body attraction is expressed with Legendre polynomials. In this work, terms up to the 4^{th} order are considered. The expression is:

$$\mathcal{R}_{3b} = \frac{\mu_{3b}}{r_{3b}} \sum_{n=2}^{\infty} \left(\frac{r}{r_{3b}}\right)^n P_n(\cos S) \tag{2}$$

where μ_{3b} and r_{3b} are respectively the perturber's gravitational parameter and distance from the Earth's centre, P_n is the n-th order Legendre polynomial and S is the planetocentric angle between the third-body and the satellite.
To study the long-term dynamics, the dependence on the fast angle θ is dropped by averaging. The potential is integrated over the satellite's mean anomaly M (related to θ), considering the orbital elements constant over one satellite's period. The computation is expressed as follows:

$$\overline{\mathcal{R}} = \frac{1}{2\pi}\int_0^{2\pi} \mathcal{R} dM \tag{3}$$

The obtained result, in the case of the third-body's potential, still depends on the fast angle θ_{3b} related to the third-body, consequently a second averaging shall be performed to filter out the short-term variations. The procedure is similar to Eq. (3), this time the computation is carried out over the third-body mean anomaly M_{3b}, as follows:

$$\overline{\overline{\mathcal{R}}} = \frac{1}{2\pi}\int_0^{2\pi} \overline{\mathcal{R}} dM_{3b} \tag{4}$$

Conversely, the Double-Averaged (DA) Earth's oblateness potential is equal to the Single-Averaged (SA) one $\overline{\overline{\mathcal{R}}}_{J_2} = \overline{\mathcal{R}}_{J_2}$.
The Hamiltonian of the considered system is expressed as:

$$\mathcal{H} = -\frac{\mu_\oplus}{2a} - \mathcal{R}_{J2} - \mathcal{R}_\odot - \mathcal{R}_\leftmoon \tag{5}$$

where $\mathcal{R}_\odot$ and $\mathcal{R}_\leftmoon$ are respectively the potentials of the Sun and the Moon. Given the constancy of the semi-major axis a, and considering the DA, the Hamiltonian depends on the 4 remaining orbital elements and on the third-body ephemerides. The Moon, in particular, features a precessing behaviour, and both its eccentricity $e_\leftmoon$ and argument of perigee $\omega_\leftmoon$ could undergo significant variations depending on the adopted frame. Since the ephemerides depend on the time t, the Hamiltonian is dependent on the following variables:

$$\overline{\overline{\mathcal{H}}} = \overline{\overline{\mathcal{H}}}(e, i, \Omega, \omega, t) \tag{6}$$

where the variables $\{e, i, \Omega, \omega\}$ are respectively the satellite's eccentricity, inclination, right ascension of the ascending node and argument of perigee.
The system's dynamics can be further reduced at this point by a third averaging operation over the node Ω:

$$\overline{\overline{\overline{R}}} = \frac{1}{2\pi}\int_0^{2\pi} \overline{\overline{\mathcal{R}}} d\Omega \tag{7}$$

The dropped dependence on the node consents to use the constancy of the Kozai parameter Θ (from Kozai [7]) to relate the eccentricity and the inclination:

$$\Theta := \left(1 - e^2\right)\cos^2 i = const. \tag{8}$$

The Hamiltonian is therefore reduced to:

$$\overline{\overline{\overline{\mathcal{H}}}} = \overline{\overline{\overline{\mathcal{H}}}}(e, \Omega, t) \tag{9}$$

At this point, if the variation of the third-body's ephemerides are neglected, the Hamiltonian expression results to be constant, hence the problem is reduced to a single-degree-of-freedom (DoF).
In this work, however, the variation of the Moon's orbital elements is considered by proposing an alternative optimisation strategy.

3. Disposal design

The Triple Average (TA) framework is exploited to compute the optimal end-of-life disposal. The design is based on the application of a single impulsive manoeuvre to accomplish the atmospheric re-entry. The target altitude $h_{p,tar}$ must be reached within the 25-year limit after the manoeuvre is applied, as imposed by the IADC (see [8]). The optimizing manoeuvre parameters are namely the impulse magnitude Δv, in-plane firing angle α, the out-of-plane firing angle β and the true anomaly of the satellite θ, which identifies where in the orbit the manoeuvre is applied. First, the satellite's orbital parameters are propagated with the TA model from the initial conditions in a fixed time period. The obtained results are then parsed on fixed manoeuvring times t_m, decided a priori. Finally, each manoeuvring point is optimized independently from one another. The overall found optimal solution will be given by the manoeuvring point associated with the lower Δv satisfying the re-entry condition.

The optimization algorithm itself is structured separately for the angles and the impulse. Following the work from Asperti [5], the optimization strategy is based on the maximization of the Kozai variation $-\Delta\Theta$, which translates the phase space topology towards higher maximum eccentricity values as shown in Fig. 10.

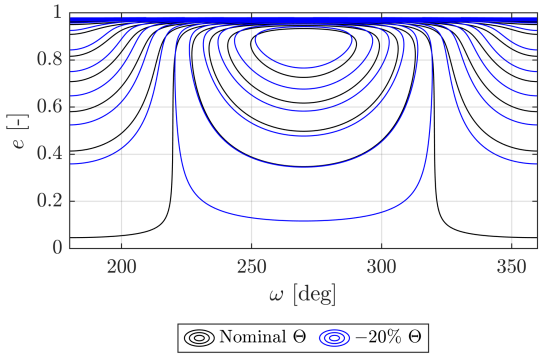

Figure 1: Modification of the phase space topology with a decrement of the Kozai parameter Θ

The expression of the variation after linearization can be written as:

$$\Delta\Theta \approx -2\cos i\sqrt{\frac{a\left(1-e^2\right)}{\mu_\oplus}}f\left(\alpha,\beta,\theta\right)\Delta v \quad (10)$$

which shows a linear dependence on both the impulse and a function $f = f(\alpha, \beta, \theta)$ embedding the dependence on the angles. This means that the optimization of the angles and the impulse can be performed separately. Regarding the angles, they are optimized by maximizing $f(\alpha, \beta, \theta)$.

The impulse optimization proposed in this work, proceeds by constructing two vectors of Hamiltonians $\mathbf{H}$ and $\mathbf{H}_{crit}$:

- In the vector $\mathbf{H}$ are stored the values of the Hamiltonians in successive time instants from t_m. Note that a simplification of the problem is made, since the orbital elements of the satellite $\{e, \omega\}$ are considered constant in this operation.
- The same is done for the values of the vector of critical Hamiltonians $\mathbf{H}_{crit}$, computed substituting the calculated $\{e_{crit}, i_{crit}\}$ to the nominal values.

The index of those two vectors embeds the information of the time instant. Those are then used inside an optimization algorithm. Between several test functions, the following one gave the best results, in synergy with a zero search algorithm:

$$\text{fun}(\Delta v) = \max\left(\mathbf{H}_{crit}(\Delta v) - \mathbf{H}(\Delta v)\right) = 0 \quad (11)$$

This optimization ensures that, at least, the values of the critical Hamiltonians are characterized by a slightly higher value. This may correspond to an actual Hamiltonian at a slightly higher eccentricity, thus granting better results with respect to the case with the neglected variation of the third-bodies' ephemerides, where the nominal Hamiltonian was imposed equal to the critical one solely at the t_m point. This imposition could not be made with a time-varying Hamiltonian.

In such a way, the overall manoeuvring parameters $\{\Delta v, \alpha, \beta, \theta\}$ are retrieved.

The other optimization design proposed in this work is a hybrid algorithm, combining the analytical angles optimization found with the maximum $-\Delta\Theta$ strategy with a local optimization algorithm for impulse minimization. This approach follows the same preliminary operations of the analytical optimization, but instead of parsing the satellite's orbital evolution with a TA model, the more accurate DA model is used. The same is used also for local optimization, im-

plementing the following cost function:

$$J = \lambda_v \left(\frac{\Delta v}{\sigma_v}\right)^2 + ... + \lambda_{h_p} \max\left[\left(\frac{h_{p,min} - h_{p,tar}}{h_{p,tar}}\right), 0\right]^2 \quad (12)$$

where the weighting and reference factor values are fixed as reported in Table 1

λ_v [-]	σ_v [m/s]	λ_{h_p} [-]	$h_{p,tar}$ [km]
1	150	100	50

Table 1: Weighting and reference factors fixed values.

This design, although computationally heavier than the analytical one, has the advantage of eliminating the frame dependence to which the TA is subjected. The time spent for the optimization is still confronted with the global optimization.

4. Case Study

The INTEGRAL satellite is used as the case study to test the optimization design algorithms. The orbital elements are integrated starting from the initial conditions on 22/03/2013, reported in Table 2 referring to the ecliptic frame, and propagated until 9 years later.

a [km]	e [-]	i [deg]	Ω [deg]	ω [deg]	θ [deg]
87720	0.8766	65.70	254.83	279.02	188.30

Table 2: INTEGRAL mission orbital elements on 22/03/2013, ecliptic frame.

The optimization computation in this work is carried out within different Laplace frames scenarios L_i, numbered as follows:

1. Lunar orbit assumed to lay in the ecliptic
2. Moon's orbital elements assumed constant (no precession considered)
3. Osculating Laplace frame (the orientation in this case is time-dependent)
4. Moon's inclination and argument of pericentre averaged
5. All Moon's orbital elements averaged

The TA propagation used in a given L_i, embeds also its assumptions. Differently from the others, L_3 exploits a rotating frame. This peculiar case requires an additional term on the Hamiltonian due to the rotation potential:

$$\mathcal{R}_{rot} = -\boldsymbol{\omega}\,(\mathbf{r} \times \mathbf{v}) \quad (13)$$

where $\boldsymbol{\omega}$ is the angular velocity vector of the osculating Laplace plane, while $\mathbf{r}$ and $\mathbf{v}$ are respectively the position and the velocity vectors of the satellite. The vector $\boldsymbol{\omega}$ is computed via central scheme difference, using the variation in time of the rotation matrix from the equatorial frame to L_3. This procedure introduces some integration errors that cumulate with time. That said, the propagation can be considered reasonably accurate if the time considered is not too extended.
Among all the cases, in Fig. 2 the evolution using L_3 was computed both in the TA and in the DA models. The results are encouraging.

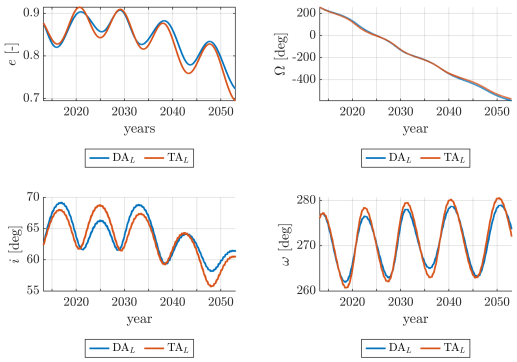

Figure 2: INTEGRAL orbital elements evolution in rotating Laplace frame (case 3) using different methods (DA, TA). In order, eccentricity e, RAAN Ω, inclination i, argument of pericentre ω.

The implementation of a rotating Laplace frame, compared to the other scenarios considered, successfully catches the missing underlying information on the system's dynamics, recovered in this model by the additional rotational potential term $\mathcal{R}_{rot}$.
The computation is therefore carried out in each presented model, and the results are compared. Starting from the global optimization results, used as the benchmark, the results are depicted in Fig. 3, where for simplicity only the impulse Δv is shown from the overall manoeuvre parameter set $\{\Delta v, \alpha, \beta\theta\}$.
The algorithm was computed within the DA model, using the cost function from Eq. (12).

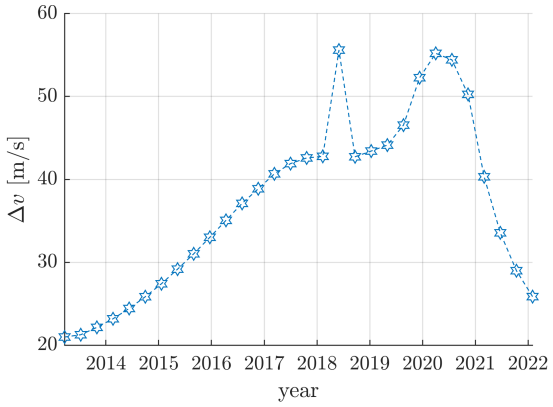

Figure 3: Optimized impulse Δv for each manoeuvring point t_m. Found with global optimization using DA in ecliptic frame.

The method is characterized by high domain "exploration" capabilities, finding accurate minimum parameters at the cost of an expensive computational burden. The overall optima set is reported in Table 3.

t_m	Δv [m/s]	α [deg]	β [deg]	θ [deg]	t_{comp} [s]
21/03/2013	20.98	-180.00	0.12	-27.39	39554.98

Table 3: Best set of manoeuvre parameters. Found with global optimization using DA in ecliptic frame.

The optimal value is found at the very first manoeuvring point, with a total computational time $t_{comp} = 11$ h.
To ease the process by allowing an on-board computational by the satellite itself, the analytical optimization design is tested. The outcomes in terms of Δv are reported in Fig. 4, where the unsuccessful re-entries within the TA model are depicted with a red marker. Note that L_5 is not present since the results in such a scenario were detached from the real system's dynamics.
The most interesting results are obtained within the L_3 frame. Only a couple of optimized manoeuvres do not reach the target, while the general tendency of the solution significantly differs from the other results. At first, the algorithm gives as best impulse for the disposal, the maximum equivalent to the constraint, which is not an optimal solution. After 2018 instead, the impulse magnitude decreases, reaching even the best result among all the inspected cases.
The overall optimal impulse found by each algorithm is reported in Table 4.

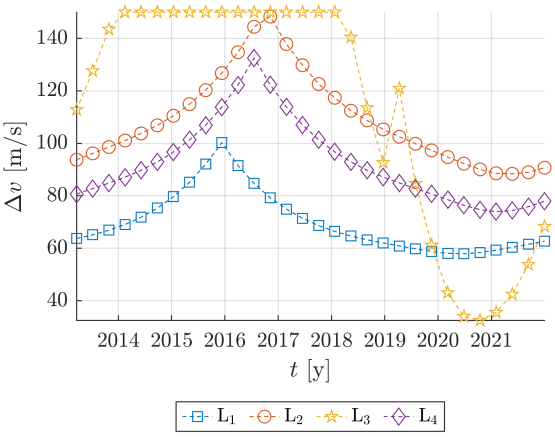

Figure 4: Optimized impulse Δv of manoeuvre paramaters for each manoeuvring point t_m. Found with Analytical time-varying $\mathcal{H}$ optimization using TA in different Laplace frames case scenarios L_i.

	t_m	Δv_{opt} [m/s]	α_{opt} [deg]	β_{opt} [deg]	θ_{opt} [deg]	t_{comp} [s]
L_1	26/06/20	57.93	176.64	-1.85	-179.63	422.42
L_2	24/05/21	88.38	-177.92	-1.11	-179.75	397.31
L_3	15/10/20	32.54	176.48	-1.84	-179.68	898.93
L_4	02/02/21	73.95	-178.03	1.09	-179.78	462.14

Table 4: Best set of manoeuvre parameters found with Analytical optimization with time-dependent $\mathcal{H}$, using TA in different Laplace frames case scenarios L_i.

The computational time is highly decremented with respect to the global optimization. Among all the results the solution which comes closest to the benchmark result is obtained within the rotating Laplace frame, and future work focusing on the exploitation of the rotating Laplace frame, looking for a best-suited analytical optimization function for that particular case may give even better results.
The other optimization design proposed in this work is the hybrid optimization. Its results are reported in Table 5. The design in this case is not carried out over the rotating frame because the integration in this frame is computationally heavier, and would nullify the proposed objective of decreasing the time spent for the optimization process.

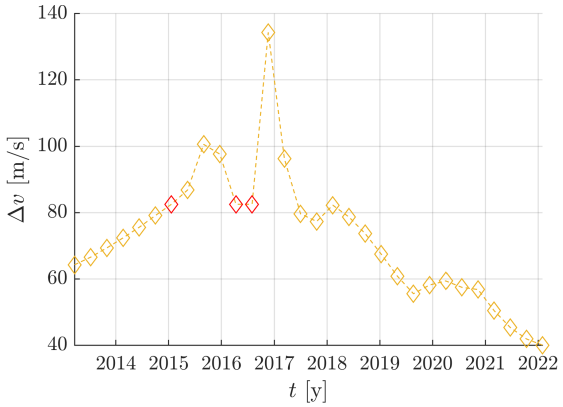

Figure 5: Optimized impulse Δv for each manoeuvring point t_m. Found with hybrid optimization.

	t_m	Δv_{opt} [m/s]	α_{opt} [deg]	β_{opt} [deg]	θ_{opt} [deg]	t_{comp}
L_1	31/01/22	42.23	132.72	-29.83	-173.03	6101.59
L_2	31/01/22	38.45	122.12	41.03	-69.95	7034.62
L_4	31/01/22	40.00	2.19	-0.59	-2.99	7001.60
L_5	11/12/21	45.50	133.09	-75.16	-173.44	9113.63

Table 5: Best set of manoeuvre parameters found with Hybrid optimization, using DA in different Laplace frames case scenarios L_i.

The optimal results show this time an acquired independence of the chosen frame. The magnitude of the impulses is more or less the same, with some minor differences. As expected, the computational time is higher with respect to the analytical, but still one order of magnitude lower with respect to the global optimization. Considering the frame L_4 as an example, the impulses found are reported in fig (5)
As shown, apart from three solutions not reaching the target altitude, a successful solution is generally found.

5. Conclusion

The exploitation of a time-varying Hamiltonian for an analytical optimization design allowed the exploitation of the rotating Laplace frame. Even if some issues were found, the result within this frame gave the minimum impulse manoeuvre amongst the considered case scenarios, still higher with respect to the optimal manoeuvre found by the global optimization algorithm, but comparable, and with a sensible computational cost reduction. Moreover, the TA model in this rotating frame allowed a more precise depiction of the system's dynamics, catching the non-periodic variations.
Regarding the Hybrid optimization design, the results demonstrated effective performance in identifying successful re-entry manoeuvres, albeit requiring higher impulses compared to the benchmark solution from global optimization. However, this was achieved with a reduced computational cost.
In light of the obtained results, future work may focus on the exploitation of the rotating Laplace frame, looking for a best-suited analytical optimization function for that particular case may give even better results.

References

[1] D. J. Kessler and B. G. Cour-Palais. Collision frequency of artificial satellites: The creation of a debris belt. *Journal of Geophysical Research: Space Physics*, 83(A6):2637–2646, 1978. doi: https://doi.org/10.1029/JA083iA06p02637.

[2] C. Colombo, E.M. Alessi, and M. Landgraf. End-of life disposal of spacecraft in highly elliptical orbits by means of luni-solar perturbations and moon resonances. *Earth*, 3 (2):2–2, 2013.

[3] C. Colombo, F. Letizia, E.M. Alessi, and M. Landgraf. End-of-life Earth re-entry for highly elliptical orbits: the INTEGRAL mission. In *Advances in the Astronautical Sciences*, volume 152, January 2014.

[4] F. Scala. Analytical design of end-of-life disposal manoeuvres for highly elliptical orbits under the influence of the third body's attraction and planet's oblateness. Master's thesis, Politecnico di Milano, 2018. Faculty of Industrial Engineering, Department of Aerospace Science and Technologies, Master in Space Engineering, Supervisor: C. Colombo, Co-supervisor: I. Gkolias.

[5] M. Asperti. Analytical design of end-of-life disposal manoeuvres in the perturbed phase space. Master's thesis, Politecnico di Milano, 2021. Faculty of Industrial Engineering, Department of Aerospace Science and Technologies, Master in Space Engineering, Supervisor: Colombo, C. Co-supervisor: X. Lu and I. Gkolias.

[6] D.A. Vallado and W.D. McClain. *Fundamentals of Astrodynamics and Applications*. Fundamentals of Astrodynamics and Applications. Microcosm Press, 2001. ISBN 9781881883128.

[7] Y. Kozai. Secular perturbations of asteroids with high inclination and eccentricity. *The Astronomical Journal*, 67:591–598, November 1962. doi: 10.1086/108790.

[8] IADC. IADC space debris mitigation guidelines, 2020. URL `https://orbitaldebris.jsc.nasa.gov/library/iadc-space-debris-guidelines-revision-2.pdf`.